A Smart Wirelessly Powered Homecage for Long-Term High-Throughput Behavioral Experiments

Byunghun Lee, *Student Member, IEEE*, Mehdi Kiani, *Student Member, IEEE*,
and Maysam Ghovanloo, *Senior Member, IEEE*

Abstract—A wirelessly powered homecage system, called the EnerCage-HC, that is equipped with multicoil wireless power transfer, closed-loop power control, optical behavioral tracking, and a graphic user interface is presented for longitudinal electrophysiology and behavioral neuroscience experiments. The EnerCage-HC system can wirelessly power a mobile unit attached to a small animal subject and also track its behavior in real-time as it is housed inside a standard homecage. The EnerCage-HC system is equipped with one central and four overlapping slanted wire-wound coils with optimal geometries to form three- and four-coil power transmission links while operating at 13.56 MHz. Utilizing multicoil links increases the power transfer efficiency (PTE) compared with conventional two-coil links and also reduces the number of power amplifiers to only one, which significantly reduces the system complexity, cost, and heat dissipation. A Microsoft Kinect installed 90 cm above the homecage localizes the animal position and orientation with 1.6-cm accuracy. Moreover, a power management ASIC, including a high efficiency active rectifier and automatic coil resonance tuning, was fabricated in a 0.35-μm 4M2P standard CMOS process for the mobile unit. The EnerCage-HC achieves a max/min PTE of 36.3%/16.1% at the nominal height of 7 cm. *In vivo* experiments were conducted on freely behaving rats by continuously delivering 24 mW to the mobile unit for >7 h inside a standard homecage.

Index Terms—Closed-loop inductive power transmission, automatic tracking, implantable medical devices, radio-frequency identification (RFID), homecage, EnerCage, Kinect.

I. INTRODUCTION

BEHAVIORAL neuroscience research on small awake animal subjects, such as rodents, has benefited from recent advances in neural interfacing technology. Neural interfaces have been traditionally hardwired to deliver power and communicate with neural recording or stimulation instruments attached to the animal body (we will refer to them as the mobile units), thereby restricting experiments that involve freely behaving animal subjects [1], [2]. These studies also require labor-intensive human operator involvement to ensure continuous and smooth flow of the experiments, which imposes a barrier to conducting long-term experiments over the span of several days, weeks, or months. In an attempt to overcome the limitations imposed by cables, several battery-powered neural recording systems have been developed [3]–[9]. Although these setups can eliminate the cables from the mobile unit, they are still not suitable for longitudinal studies due to the limited lifetime of the batteries, which also add to the animal payload. Researchers have to make compromises between the duration of the experiment and how much weight the animal can carry before it affects its natural behavior and bias the results.

In order to address these limitations, a few wirelessly-powered systems have been developed to either directly power the mobile unit or recharge the batteries during the experiment [10]–[15]. However, these systems suffered from poor power transfer efficiency (PTE) because the coil geometries were not optimized. Moreover, they continuously powered the entire homecage, as opposed to where the animal was located, reducing the flux linkage between the transmitter (Tx) and receiver (Rx) coils, resulting in lower coupling coefficient and transmission of more power for delivering sufficient power to the mobile unit. In an attempt to circumvent these problems, smart wirelessly-powered systems have been reported, which can significantly improve the PTE [16]–[22]. In these systems, batteries on the mobile units have been eliminated or replaced by smaller super capacitors, and an array of coils at the bottom of the experimental arena that are automatically selected based on the position of the animal subject to couple with the Rx coil in the mobile unit. As a result, the new systems can achieve higher PTE and dissipate less heat for the same amount of power received at the mobile unit. As an alternative, a single Tx coil mechanically moving on XY-rails was also reported in [23]. Although these systems can achieve high PTE and operate at low temperature, they are too bulky to be integrated with the standard homecage (HC) in a way that high throughput experiments can run in parallel over extended periods of time inside the animal research facilities without occupying the lab space and limited human resources of research laboratories.
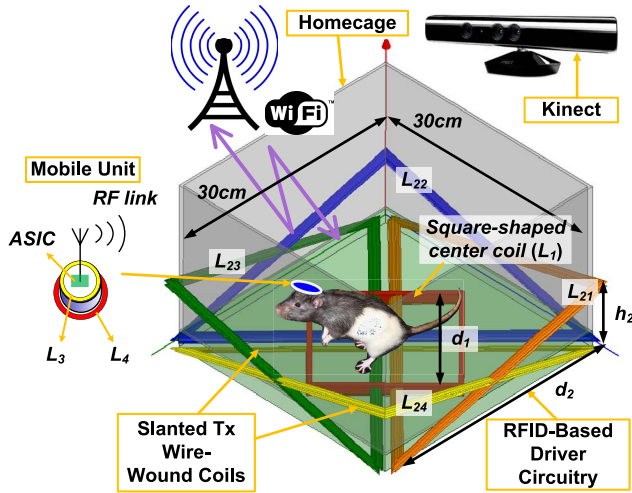
Fig. 1. 3D rendered view of the EnerCage-HC system with one square-shaped WWC at the bottom of the homecage and four overlapping slanted triangular WWCs on the corners. A custom ASIC receives power in the mobile unit and generates a stable supply for the sensing blocks and bidirectional RF data link. Animal position and orientation are tracked in real-time by a Microsoft Kinect.

Moreover, the animal tracking resolution and quality in the earlier work were not sufficient for behavioral experiments.

Tracking animal subjects to analyze the locomotion has been separately studied on different animal species including rodents [24]–[28]. Automated locomotion measurement using computer vision can improve accuracy and significantly lower the cost of labor, thus it is rapidly growing [29]–[33]. Microsoft Kinect® is a popular high-precision and low-cost imager that is equipped with infrared depth (IR-3D) and Red-Green-Blue (RGB-2D) cameras, allowing animal tracking in both bright and dark conditions. This is particularly important for nocturnal animal species, which include most rodents. Kinect® has been recently adopted in a few automated locomotion tracking experiments [34], [35]. However, only the depth camera has been previously used for tracking the subject's position in real time.

In this paper, we present a wirelessly-powered smart homecage, called the EnerCage-HC, which is conceptually shown in Fig. 1, and includes: 1) a compact and geometrically-optimized array of wire-wound coils (WWCs) with one central WWC at the bottom of the cage and four overlapping slanted WWCs on the corners of the cage to form 3- or 4-coil links and generate a homogeneous high-PTE space inside the homecage ($30 \times 30 \times 17$ cm^3) [36], thanks to, 2) a closed power control loop (CPCL) that can dynamically compensate for coupling distance and load variations due to animal movements and implant functions (e.g. stimulation on/off), respectively, 3) an automated real-time behavioral tracking mechanism based on 2D and 3D imaging with Microsoft Kinect®, and 4) a custom-designed coin-sized mobile unit that includes two Rx coils and an efficient power management integrated circuit (PMIC).

The EnerCage-HC system has a different structure and serves a different purpose compared to our previously-reported EnerCage system in [19], in terms of using a set of slanted wired-wound coil structure instead of an array of overlapping printed spiral coils (PSC). It also benefits from reduced number of cables by using WiFi instead of Ethernet, a power management ASIC in the mobile unit for smaller size and higher efficiency, safety functions during *in vivo* experiments, and accurate animal subjects tracking features. Unlike the original EnerCage that was offering large wirelessly powered experimental arenas, the EnerCage-HC is intended for automated, high throughput, and long-term experiments in a large number of parallel cages that can be located in standard racks in animal research facilities without requiring labor intensive supervision or occupying precious laboratory space. In section II, the EnerCage-HC system architecture is introduced. The coil design and optimization are presented in section III. The optical tracking is discussed in section IV. The power management ASIC has been described in section V, followed by the *in vivo* measurement results in section VI and conclusions.

II. ENERCAGE-HC SYSTEM ARCHITECTURE

Fig. 1 shows a rendered view of the proposed EnerCage-HC system. The square-shaped center-WWC (L_1) at the bottom of the cage can directly form a 3-coil power transmission links with two coils (L_3, L_4) that are embedded in the mobile unit when the subject is located in the center of the cage. All other WWCs ($L_{21} \sim L_{24}$) are open-circuit. L_1 can also form a 4-coil link with one of the triangular-shaped overlapping slanted WWCs ($L_{21} \sim L_{24}$) when the subject is located near a corner of the homecage by shorting that particular WWC with a resonant capacitor to form a series high-Q LC-tank. The sizes of the central and triangular WWCs are d_1 and d_2, respectively, and the tips of the triangular WWCs are elevated by h_2.

In this system, multi-coil resonance-based inductive link not only increases the PTE compared to similar sized 2-coil links but also reduces the required number of power amplifiers (PA) to only one, which in turn reduces the system complexity, cost, and dissipated heat. Hence, only L_1 is driven by a class-C PA at $f_p = 13.56$ MHz, and $L_{21} \sim L_{24}$ simply form high-Q LC-tanks. The PA is driven by an RFID reader (TR7960, Texas Instruments, Dallas, TX). The CPCL changes the PA supply voltage (V_{DD_Tx}) based on the information it receives about the mobile unit rectifier output voltage, V_{RECP} in Fig. 2, which is back telemetered via load shift keying (LSK) by shorting the $L_4 C_4$-tank [37]. In this prototype, in order to monitor the system operation, V_{RECP} is also divided down, digitized, and wirelessly sent back to the central PC station by the mobile unit MCU and its built-in 2.4 GHz transceiver. This data is used for monitoring the mobile unit operation and ensuring the EnerCage-HC system functionality. The central PC station is also responsible for processing the Kinect images to detect and report the animal position in each EnerCage-HC in real time. This information is then used to switch $L_{21} \sim L_{24}$.

A. Stationary Unit

Fig. 2 shows a detailed block diagram of the prototype EnerCage-HC system. The stationary unit is composed of a coil array (L_1, $L_{21} \sim L_{24}$), a controller module, CPCL,
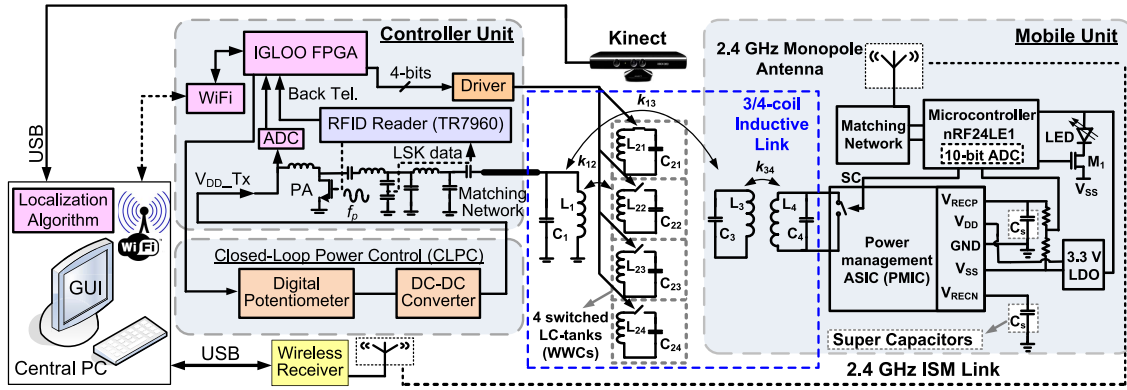
Fig. 2. Block diagram of the EnerCage-HC system for automated, high throughput, and long-term awake animal experiments in a standard homecage. The controller unit has an FPGA to process the position data from the PC and activate the WWCs in a way that they form 3- and 4-coil power transfer links based on the animal position. The PA output power is dynamically controlled in a closed loop based on the received power at the mobile unit. All the acquired information and system operating status are wirelessly transmitted to the PC station. The mobile unit on the animal body receives power inductively, generates a stable supply voltage through a power management ASIC, and communicates with the RFID reader via load shift keying (LSK). An LED blinking at 50 Hz with 4% duty cycle helps with 2D/3D Kinect localization and indicates both the animal location and orientation (i.e., where it is heading) inside the homecage.

a Microsoft Kinect[®] for optical tracking, and a central PC station with a graphical user interface (GUI). A field-programmable gate array (FPGA) receives the animal coordinates from the PC via a WiFi link, and use them to close- or open-circuit $L_{21}C_{21} \sim L_{24}C_{24}$ tank circuits. The RFID reader not only drives the class-C PA, but also recovers the back telemetry (BT) data from the PMIC. The V_{DD_Tx} is dynamically controlled by the CPCL from 4.5 V to 20 V in 256 steps based on the BT data to compensate for any coil coupling and loading variations [37]. In the EnerCage-HC system, 1-bit BT data is used to increase or decrease the V_{DD_Tx}. The received BT pulses indicate that the received power in the mobile unit is sufficient, where the coupling between stationary and mobile unit is strong enough. The received BT pulses are oversampled by the FPGA to decrease the V_{DD_Tx} at the rate of 320 steps/s by controlling a digital potentiometer (AD5160) in the feedback loop of the DC-DC converter (LT1370). In the absence of BT pulses, the FPGA increases the V_{DD_Tx} at the same rate [37].

B. Mobile Unit

The mobile unit, shown on the right side of Fig. 2, is equipped with the PMIC, two super-capacitors, a 3.3 V low dropout regulator (LDO), an LED tracer, and an MCU (nRF24LE1, Nordic Semiconductor, Norway). The PMIC includes two active rectifiers to generate both positive V_{RECP} and negative V_{RECN} for bipolar stimulation [38], two LDOs to generate $V_{DD} = 2$ V and $V_{SS} = -2$ V, an automatic resonance tuning (ART) block, and LSK circuitry. An off-chip LDO is used to generate a separate 3.3 V supply voltage for the MCU. V_{RECP} is divided by two and digitized by the MCU built-in 10-bit ADC. When V_{RECP} is higher than 2.3V, the MCU sends narrow pulses to the PMIC at 3 kHz, which are sharpened ($\sim$0.4 μs) before shorting the L_4C_4-tank as briefly as possible to close the power control loop with minimal degradation of the PTE. The duty cycle of the BT short-circuit pulses is only 0.1% significantly minimize the power loss. The MCU also turns on/off transistor M_1 at 50 Hz with 4% duty cycle to blink a green LED for optical

tracking of the mobile unit. Two 0.21 F super capacitors, following V_{RECP} and V_{RECN}, supply the mobile unit when the received power is interrupted by $>80°$ tilting of the mobile unit or >18 cm coupling distance from the bottom of the homecage. These thresholds are experimentally determined when the PTE has reached a low level that even the maximum PA power in the EnerCage-HC system (7 W) is not sufficient to provide enough power to the mobile unit.

C. Graphical User Interface

All acquired information, such as V_{RECP}, V_{DD_Tx}, and system operating status e.g. WiFi and MCU 2.4 GHz link connectivity, along with the Kinect images are collected by the central PC from each EnerCage-HC system to be used in the signal/image processing algorithm and the GUI. The subject coordinates are sent from the PC to the FPGA using the User Datagram Protocol (UDP), while two-way communication through TCP/IP is used for monitoring the V_{DD_Tx}. The same link is used to reduce V_{DD_Tx} to 4.5 V when no mobile unit is detected in the homecage. The GUI displays a real time color video of the homecage, position of the animal and mobile unit in the cage, the total distance that the animal has traveled, the processed depth image, the active WWC, the connection status, V_{RECP}, and V_{DD_Tx}. The GUI can also save the acquired data in text and movie formats.

III. MULTI-COIL LINK OPTIMIZATION FOR ENERCAGE-HC

Fig. 3 shows how utilizing 3/4-coil links eliminates the need to drive the triangular WWCs, while increasing the PTE by decoupling the loosely-coupled L_2-L_3 link from the source and load impedances [39]. When the mobile unit is in the center of the homecage, only L_1 is driven to form a 3-coil link, while the other WWCs are open-circuit. The PTE of a 3-coil link can be found from [40].

$$\eta_{3-coil} = \eta_{13} \cdot \eta_{34}$$
$$= \frac{(k_{13}^2 Q_1 Q_3) \cdot (k_{34}^2 Q_3 Q_{4L})}{[(1 + k_{13}^2 Q_1 Q_3 + k_{34}^2 Q_3 Q_{4L}) \cdot (1 + k_{34}^2 Q_3 Q_{4L})]}.$$
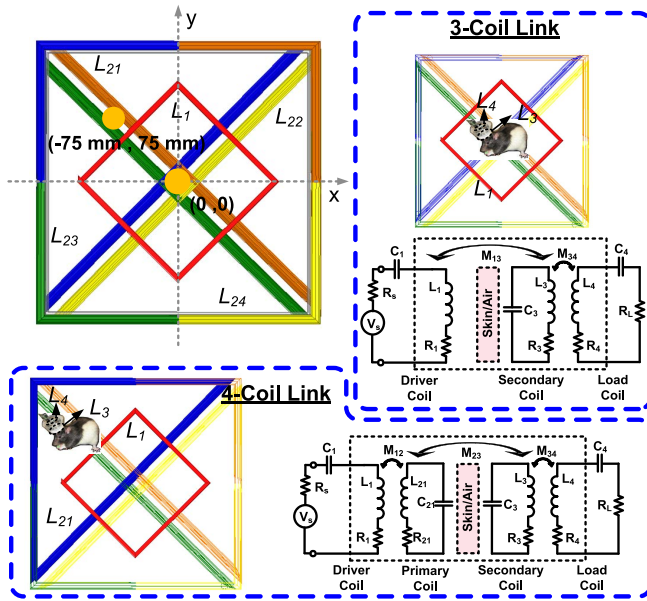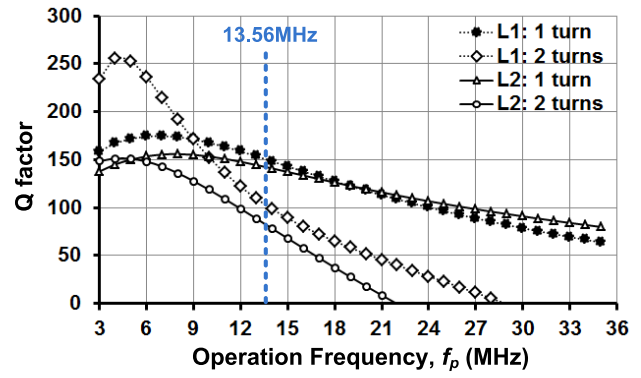$$(1)$$

Fig. 3. WWC switching to form 3- and 4-coil inductive links with the mobile unit while only driving L_1 (inactive coils are light colored).

Fig. 4. Simulation results of 3/4-coil link optimization for the EnerCage-HC system: (a) Q-factor versus f_p for different number of turns in L_1 and L_2, (b) optimal L_1 geometry for homogeneous 3/4-coil PTE, and (c) 4-coil PTE distribution on the corner of the homecage with $h_2 = 6$ cm, 8 cm, 10 cm, and 12 cm at a nominal height of $d_{23} = 7$ cm.
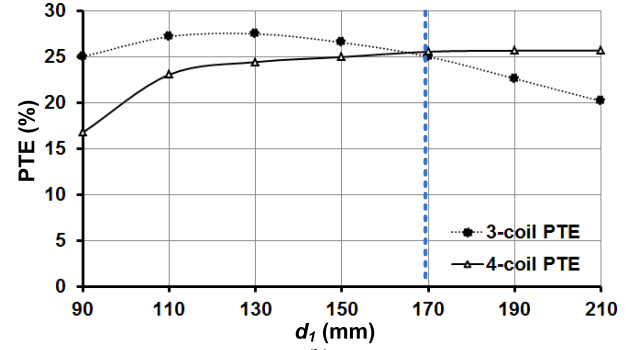
However, when the mobile unit is on the corners of the cage, the closest WWC ($L_{21} \sim L_{24}$) is shorted with a capacitor, which resonates at 13.56 MHz with the Tx, to form a 4-coil link. In a 4-coil link, the PTE can be written as [40] (2) as shown at the bottom of this page.

The quantitative model and comprehensive circuit-based analysis describing the power transmission in 4-coil inductive links are described in [39] and [40]. The WWC geometries are optimized to provide homogeneous PTE in the worst case coil misalignments.
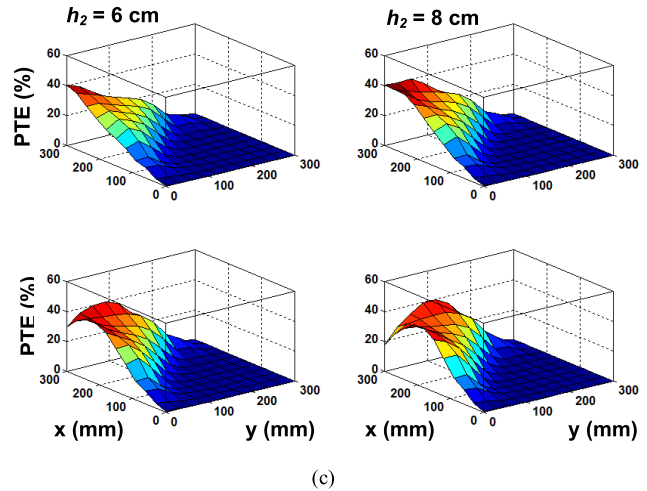
To reduce the size and weight of the mobile unit, which is carried in the headstage or a backpack, the diameter and width of L_3, i.e. D_{o3} and W_3, were limited to 2.5 cm and 0.64 mm, respectively, to be about the size of a U.S. quarter. Under the 300 Ω loading condition, which is corresponding to 24 mW of power consumption in the mobile unit, to maximize Q_3 for L_3, $n_3 = 2$ was chosen based on the HFSS simulations. The 24 mW power was chosen in this prototype as a level that is sufficient for the majority of state-of-art neural recording and stimulation devices [7]. The CPCL dynamically controls the V_{DD_Tx} to compensate for any load variations in the mobile unit. In order to embed the Tx coils inside the body of the homecage the width of the wire used in the Tx coils was limited to the thickness of the homecage. The AWG10 ($W = 2.59$ mm) wire was chosen for L_1 and $L_{21} \sim L_{24}$ to achieve the highest Q. Fig. 4a shows the HFSS simulation results of Q_1 and Q_2 vs. f_p for $n_{1,2} = 1$ turn and 2 turns. In these simulations, L_1 was square shaped with an estimated $d_1 = 19$ cm, and L_2 had an isosceles triangular shape with $d_2 = 30$ cm and $h_2 = 7$ cm (see Fig. 1). L_1 has a square shape

to increase its overlap area with $L_{21} - L_{24}$, which is directly proportional to their coupling coefficient. It is clear from these simulations that at $f_p = 13.56$ MHz in the industrial-scientific-medical (ISM) band, $n_1 = n_{21-24} = 1$ provides higher Q_1 and Q_2.

In optimizing d_1, we noticed that the common optimization algorithm in [40] leads to a smaller d_1 with higher PTE at

$$\eta_{4-coil} = \eta_{12} \cdot \eta_{23} \cdot \eta_{34} = \frac{(k_{12}^2 Q_1 Q_2) \cdot (k_{23}^2 Q_2 Q_3) \cdot (k_{34}^2 Q_3 Q_{4L})}{[(1 + k_{12}^2 Q_1 Q_2) \cdot (1 + k_{34}^2 Q_3 Q_{4L}) + k_{23}^2 Q_2 Q_3] \cdot [1 + k_{23}^2 Q_2 Q_3 + k_{34}^2 Q_3 Q_{4L}]} \tag{2}$$

TABLE I
COIL SPECIFICATIONS FOR THE PROTOTYPE ENERCAGE-HC SYSTEM

Parameters	Value
Tx wire-wound coil (L_1)	Diameter = 17 cm Wire width = 2.59 mm (AWG10) Number of turns = 1 Inductance = 0.716 μH Quality factor = 150.3
Tx wire-wound coil (L_2)	d_2 = 28 cm, h_2 = 8 cm Wire width = 2.59 mm (AWG10) Number of turns = 1 Inductance = 0.890 μH Quality factor = 154
Rx wire-wound coil (L_3)	Diameter = 2.5 cm Wire width = 0.64 mm (AWG22) Number of turns = 2 Inductance = 0.48 μH Quality factor = 136
Rx Litz wire-wound coil (L_4)	Diameter = 1 cm Wire diameter = 0.25 mm Number of turns/strands = 6/44 Inductance = 5.8 μH Quality factor = 12
L_2-L_3 nominal distance (d_{23})	7 cm
Nominal load (R_L)	300 Ω (~24 mW)
Operation frequency (f_p)	13.56 MHz

the center of L_1 in the 3-coil arrangement. However, that will also reduce the overlap between L_1 and $L_{21} \sim L_{24}$ coils, resulting in lower k_{12} and lower PTE in the 4-coil arrangement. Moreover, the powered area in the center of the homecage is also reduced by decreasing d_1, negatively affecting the homogeneity of the PTE across the homecage. Fig. 4b shows the simulated 3- and 4-coil PTE vs. d_1 at L_2-L_3 nominal distance of $d_{23} = 7$ cm when the Rx coil was located at the center of the homecage (0, 0) for the 3-coil and in the center of a triangular WWC (-75 mm, 75 mm) for the 4-coil link (see orange spots Fig. 3). Starting from 9 cm, as d_1 becomes larger, k_{12} is increased and PTE for the 4-coil link also increases. However, if d_1 becomes much larger than its optimal size for the 3-coil link, its PTE decreases due to reduced k_{13}. To create a homogeneous PTE at the coils' switching points, d_1 was selected as 17 cm, based on the simulations in Fig 4b.

To determine the L_2 triangular geometry, d_2 was chosen 28 cm, slightly less than the length of each side of the homecage (30 cm), to offer maximum overlap with L_1 but avoid overlapping among four WWCs at the center of the homecage considering the thickness of the coil wires (see the top view in Fig. 3). h_2 is key in determining the distribution of the 4-coil PTE at the corners of the homecage, where the animal tends to stand up and create a worst case scenario for power transmission from a central WWC at the bottom of the cage. Fig. 4c shows the simulated distribution of the 4-coil PTE inside the homecage for the nominal height of $d_{23} = 7$ cm when h_2 is changed from 6 cm to 12 cm in the nominal loading condition of 300 Ω. It can be seen that by increasing h_2 the high PTE region tends to move toward the center of the cage, while PTE at the corners drop. Therefore, to achieve a homogeneous PTE distribution at the corners of the homecage, $h_2 = 8$ cm was chosen, the height at which the peak PTE starts to drop. The PTE distribution is affected by L_3 and L_4 geometries and orientations, but not by the
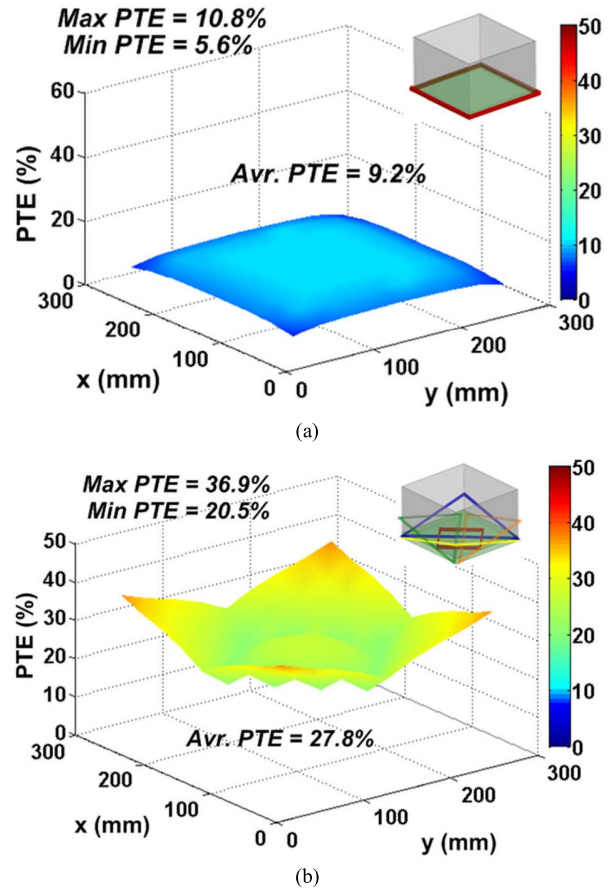
Fig. 5. Simulation results of the PTE distribution inside the homecage at the nominal height of $d_{23} = 7$ cm for (a) a single WWC [12] and (b) the proposed EnerCage-HC system.

loading condition. The PTE in the EnerCage-HC is reduced if the loading condition is out of the nominal condition. However, the CLPC dynamically adjusts the Tx power to ensure that the headstage receives sufficient power even in suboptimal loading or positioning conditions.

The geometry of L_4 was optimized as the last step for $d_{23} = 7$ cm, based on the coil optimization procedure in [40]. The nominal loading was considered to be 300 Ω, corresponding to ~24 mW power consumption in the mobile unit. L_3 and L_4 are concentric. The inductance values of L_3 and L_4 are decided by their number of turns and diameter. L_4 has a lower Q-factor compared to L_3 because the diameter of the litz wire in L_4 is much smaller than the solid wire used in L_3. Also L_4 has higher number of turns because according to our coil design, despite its smaller size, it should have a higher inductance [40]. The optimal EnerCage-HC coil geometries are summarized in Table I. The coil design is optimized for the most common conditions, i.e. a horizontal mobile unit at a nominal height of 7 cm above the bottom of the cage. The other conditions will be taken care of by the CPCL, which dynamically adjusts the Tx power to ensure the mobile unit functionality.

Figs. 5a and 5b compare the simulated PTE distribution inside the homecage at a nominal height of 7 cm when a single large WWC encompasses the bottom of the cage (see [12]) vs. our proposed 5-coil design, shown in Fig. 1, respectively.
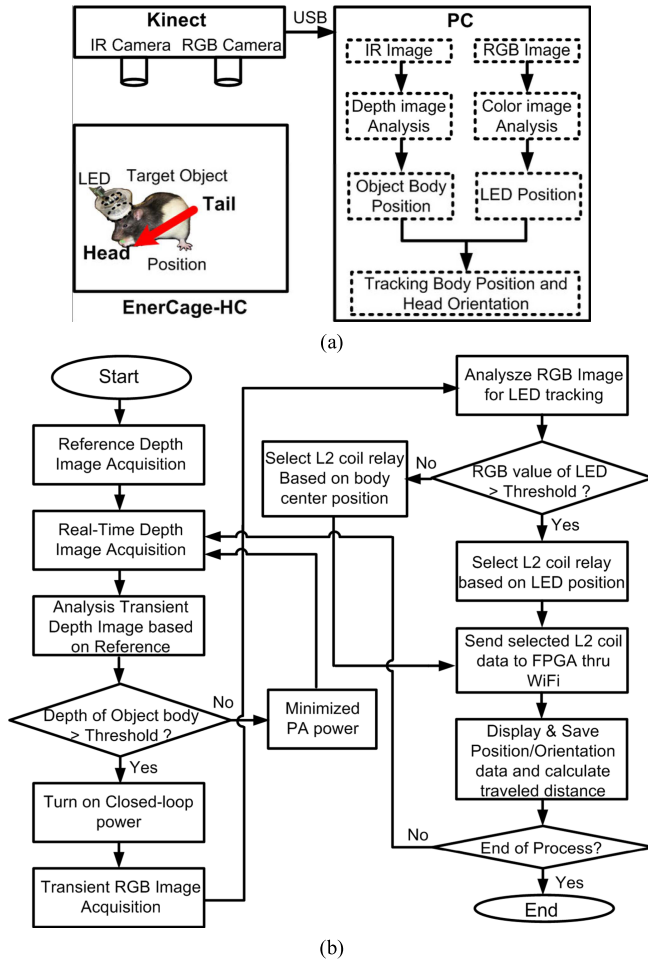
Fig. 6. Data flow diagram and flowchart of the tracking mechanism in EnerCage-HC. (a) EnerCage-HC system uses data from both RGB and IR images from the Kinect, and detects the head and body positions separately. (b) Flowchart of the software running on the PC shows how the RGB and IR images are used for real time animal tracking.
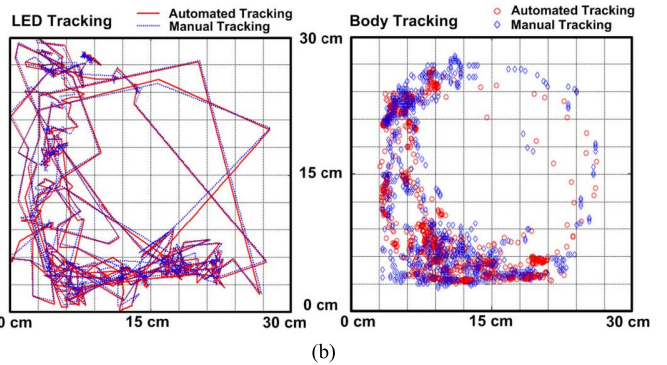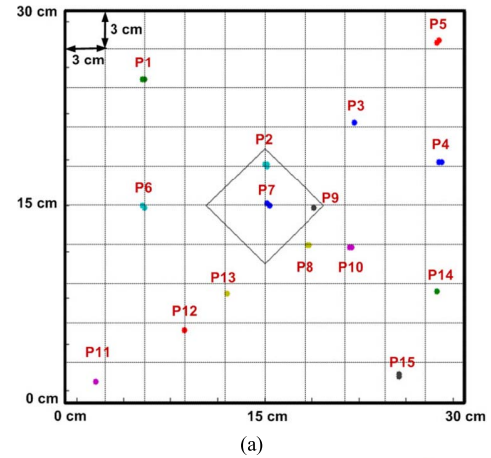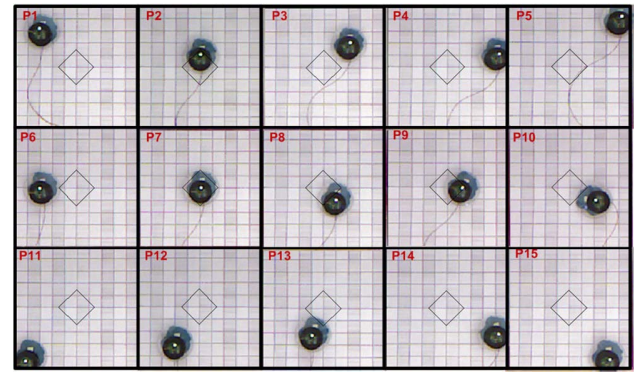

Fig. 7. Validation of the automated tracking in the EnerCage-HC system: (a) sample images of 15 random positions (P1-P15) for the LED tracking on the checker board during 3 min and (b) automated tracking versus manual tracking for a 20 min *in vivo* experiment (Left: LED and Right: body center tracking).

The conclusions from these simulations are: 1) The PTE in the corners of the EnerCage-HC is significantly higher than the single WWC design, thanks to the overlapping slanted WWCs ($L_{21} \sim L_{24}$), both when the mobile unit is held horizontally and vertically, which happen when the animal is walking on the bottom or climbing the walls of the homecage, respectively; 2) The average PTE in the EnerCage-HC is 27.8%, which is three times higher than the 9.2% average PTE of a single WWC; 3) The PTE distribution in the EnerCage-HC is considerably more homogeneous than the single WWC because the maximum PTE variation inside the homecage is 23.8% of the average PTE in the EnerCage-HC vs. 56.5% in the single WWC homecage.

IV. 2D/3D OPTICAL ANIMAL SUBJECT TRACKING

Using Kinect provides a unique opportunity to utilize both the IR depth (3D) and RGB (2D) cameras for tracking the animal subject. Another advantage of an IR-based system is its ability to track subjects even in the dark environments, which is quite helpful when experimenting with nocturnal species that include the majority of rodents. Moreover, utilizing both

IR and RGB cameras in the EnerCage-HC, aided with an LED tracer on the headstage, enables recognition of the animal subject orientation (determining its head from tail), which is important in behavioral tracking [41], [42].

A. Automated Tracking

Fig. 6 shows the hardware and software diagrams of the tracking algorithm in the EnerCage-HC system. The Kinect was installed at ~90 cm above the homecage to easily cover the 30×30 cm^2 area of the homecage. The collected depth and RGB images from the Kinect were transferred to PC via USB, as shown in Fig. 6a. The real-time depth image from Kinect was compared to a reference depth image, taken when the animal subject was not present, to find the animal subject
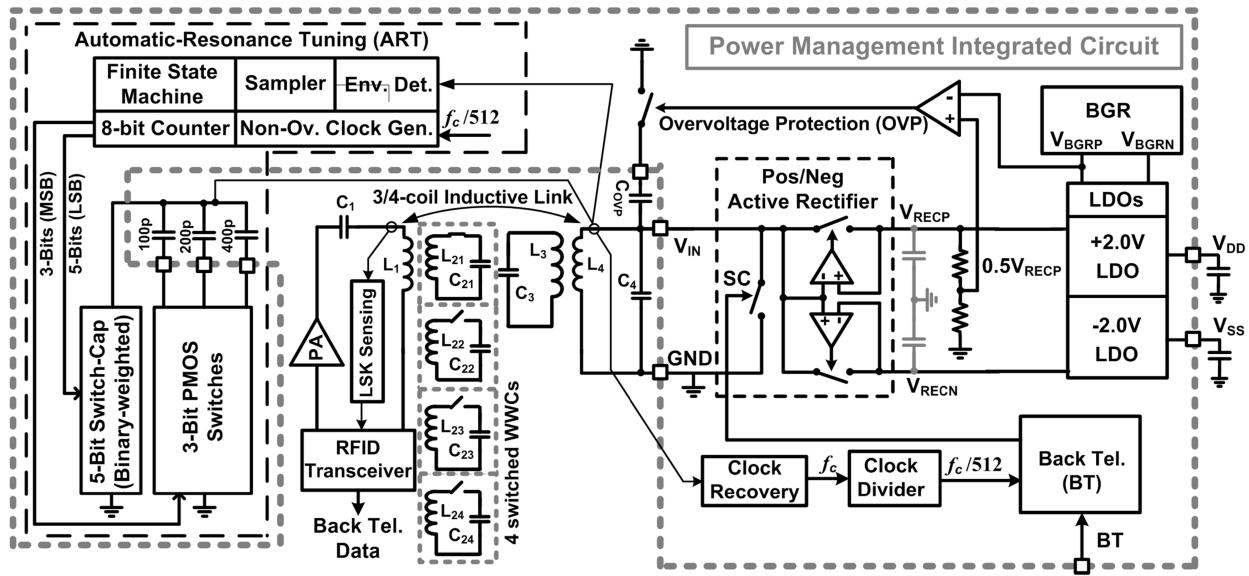
Fig. 8. Block diagram of the efficient power management integrated circuit (PMIC) in the mobile unit, which is equipped with automatic resonance tuning (ART) mechanism and back telemetry to dynamically tune the L_4C_4-tank at the 13.56 MHz carrier frequency and close the power control loop, respectively.

in the cage. The software algorithm projects the depth image voxels over a 2D plane, and indicates the areas that have higher value than a predefined detection threshold. Then, the center of the animal outline is found from the projected image to identify the center of the subject body. If the measured depth of the object is less than the threshold, the software concludes that the animal is not present in the cage, and reduces the PA power to its minimum by setting $V_{DD}\_Tx = 4.5$ V to reduce the dissipated power.

When the algorithm finds the center of the subject body, it activates the CPCL to provide sufficient amount of power to the mobile unit. It then analyzes the RGB image to find the LED indicator. At startup, when the mobile unit is not powered and the LED is off, $L_{21} \sim L_{24}$ are controlled based on the body position extracted from the depth image. When the LED indicator starts blinking, the position of the LED indicator is detected from the RGB image and combined with the center of the body to not only activate one of $L_{21} \sim L_{24}$ coils but also indicate the subject orientation.

With more advanced image processing, we are trying to pinpoint the position of the rat head directly from Kinect the 3D image. When that algorithm is fully functional, there will be no need for an additional LED localization. By tracing the acquired positions, the accumulated distance that the subject has traveled can be calculated in real time. The process for automated tracking, shown in Fig. 6, takes ∼50 ms, including the 30 Hz frame rate of the Kinect. It also depends on the performance of the central PC station. Considering relatively low speed of the animal subject movements within the homecage (30∼70 cm/s) [43] and the presence of the super capacitors in the mobile unit, the tracking mechanism in the EnerCage-HC is fast enough to provide the animal position for switching $L_{21} - L_{24}$ to power the mobile unit. All of the acquired data during the experiment is displayed on the PC screen, and saved in the PC station for post processing.

B. Validation

Fig. 7 compares the automated and manual tracking results within the EnerCage-HC. A checker board with 3 cm grid was used to manually place the mobile unit in a known position inside the homecage. Fig. 7a shows the images of 15 random mobile unit positions on the checker board compared with the automatic tracking data collected in 3 min at each position (P1 to P15). The maximum time jitter for the optical tracking was 20 ms in this test. The maximum position error was measured 1.6 cm near the corners, where the large viewing angle from the Kinect lens is the main source of inaccuracy. Fig. 7b shows the comparison between automatic (red) and manual frame-by-frame (blue) tracking of a freely behaving rat (17 cm long) from the recorded video in an *in vivo* experiment, which details are presented in section VI. We randomly selected 20 min of the recorded experiment video, and manual tracking was performed by a human observer watching the recorded video to identify the position of the LED and center of body. It can be seen from Fig. 7b that the automated tracing of the LED indicator is in good agreement with manual tracking with maximum localization error of 1.3 cm. However, since determination of the manual body center is somewhat subjective, the automated and manual tracking results are not overlapping as well as the LED tracking. Nonetheless they show similar trends.

V. POWER MANAGEMENT IC IN THE MOBILE UNIT

To increase the overall power efficiency of the EnerCage-HC system and establish a communication link between mobile and stationary units for the CPCL, while maintaining small size and volume of the mobile unit, a custom PMIC was designed. Fig. 8 shows the PMIC block diagram, along with its off-chip components that are presented outside the gray dashed box. The AC signal across the Rx L_4C_4-tank, which is tuned at $f_p = 13.56$ MHz, is rectified by the positive/negative rectifier. The rectifier outputs,
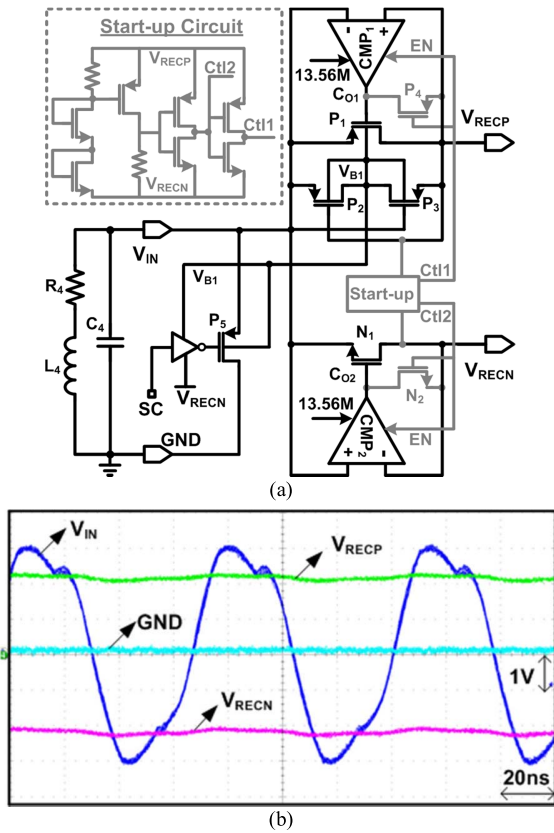
Fig. 9. Active rectifier in the PMIC [45]. (a) Circuit diagram of the positive/negative active rectifier with startup. (b) Measured waveforms at 13.56 MHz. The measured PCE was 74.3% when $R_L = 600\ \Omega$ was connected between $V_{RECP} = 2.3$ V and $V_{RECN} = -2.3$ V.
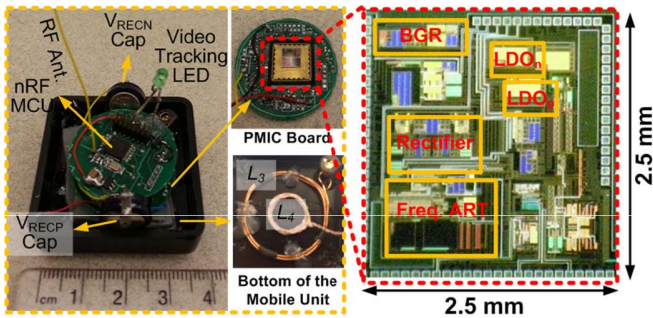

Fig. 10. The mobile unit prototype including the PMIC, an nRF MCU, and LED indicator. The PMIC was fabricated in TSMC 0.35-μm 4M2P standard CMOS process, occupying 3.5 mm^2.

$V_{RECP} = 2.3$ V and $V_{RECN} = -2.3$ V, are then applied to two LDOs, which create stable $V_{DD} = 2$ V and $V_{SS} = -2$ V. An automatic-resonance tuning (ART) block ensures that the L_4C_4- tank is always tuned at $f_p = 13.56$ MHz despite the effects of packaging, implantation, or animal proximity to large conductive objects, such as the transmitter coils.

The ART sweeps a 5-bit binary-weighted on-chip (3 pF, 6 pF, 12 pF, 24 pF, 48 pF) and a 3-bit binary-weighted off-chip (100 pF, 200 pF, 400 pF) capacitor bank, resulting in 0-800 pF capacitance change across the L_4C_4-tank with 3 pF resolution. The ART sweeps the 8-bit capacitor bank, which are connected to an 8-bit counter, in a certain
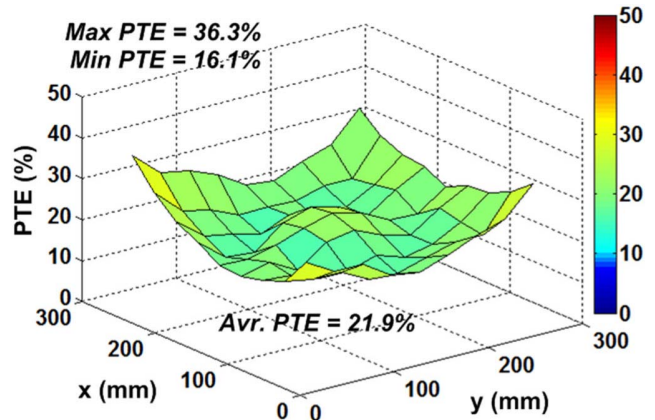
Fig. 11. Measured PTE distribution inside the EnerCage-HC.
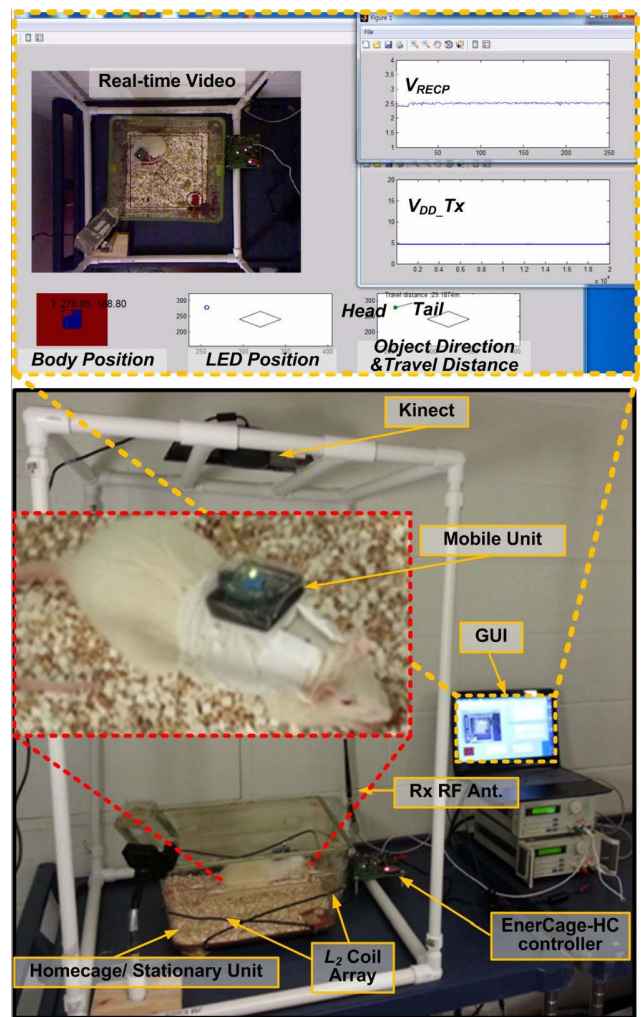
Fig. 12. *In vivo* experimental setup for the EnerCage-HC prototype. In this experiment, the rat was freely moving around the cage for 7 hour and 20 min.

direction (up or down) until the envelope of the carrier across the L_4C_4-tank, V_{ENV}, drops by 100 mV. Then the direction of the sweep changes until V_{ENV} again drops by 100 mV. This up/down cycle ensures that the L_4C_4-tank remains tuned around $f_p = 13.56$ MHz with a fluctuating small offset. The ART finds the optimal capacitance value in less than 3 ms

Fig. 13. *In vivo* experimental results showing the mobile unit positive rectifier voltage, V_{RECP}, and the transmitter PA supply voltage, V_{DD_Tx}, during $\sim$7 hrs. The CLCP increased the transmitted power, which is in proportional to V_{DD_Tx}, when the rat moved to low PTE areas or stand up as shown in inset $t < 14817$ s, and decreased V_{DD_Tx} when the mobile unit was close to the homecage surface or high PTE areas as shown in the inset $t > 14817$ s.

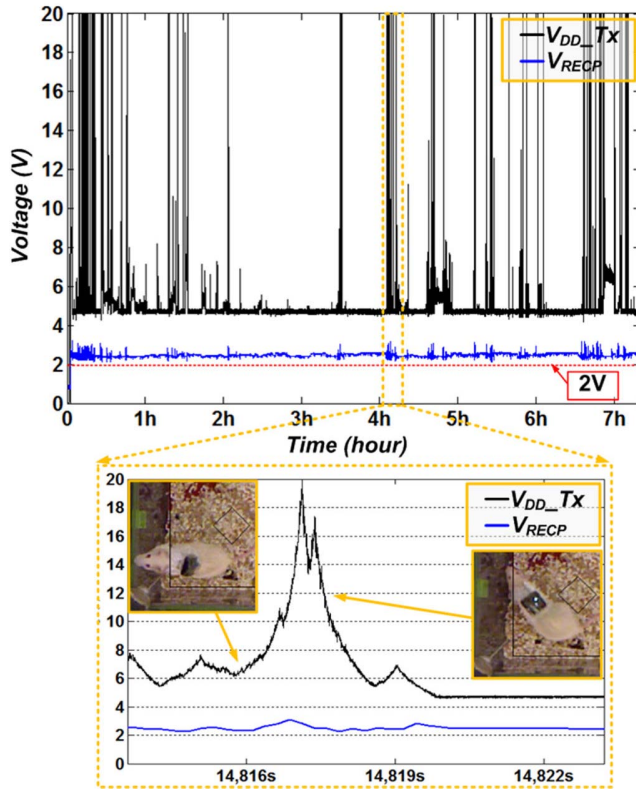when it only utilizes its 5-bit on-chip capacitors. Therefore, animal movements during this time does not effect on the ART operation. Considering the fact that the coupling between the Tx and Rx coils can become too strong, the PMIC is equipped with an over-voltage protection circuit. A hysteresis comparator detunes the L_4C_4-tank by adding $C_{ovp} = 1$ nF in parallel when $V_{RECP} > 2.6$ V to protect the PMIC from large input voltages. The PMIC chip is also equipped with back telemetry circuit to short the L_4C_4-tank with sharp pulses ($\sim$0.4 μs) for sending the V_{RECP} information for the CPCL. Additional details about the PMIC can be found in [44].

Fig. 9a shows a simplified schematic diagram of the active rectifier, consisting of the PMOS and NMOS pass transistors, which are driven by two high-speed offset-controlled comparators [45]. The startup circuit monitors V_{RECP}/V_{RECN} and sets CTL = 0 when V_{RECP}/V_{RECN} are low. At startup, P_1 and N_1 transistors are diode-connected and form a passive rectifier, which charges V_{RECP}/V_{RECN} regardless of the comparators' status up to the point that V_{RECP} and V_{RECN} reach a stable minimum level (± 1 V). Then CTL toggles to enable the active rectifier to operate normally. Fig. 9b shows measured input/output waveforms in the positive/negative rectifier at 13.56 MHz. The measured rectifier power conversion efficiency (PCE) was 74.3% when $R_L = 600$ Ω was connected between $V_{RECP} = 2.3$ V and $V_{RECN} = -2.3$ V.

(a)

(b)

(c)
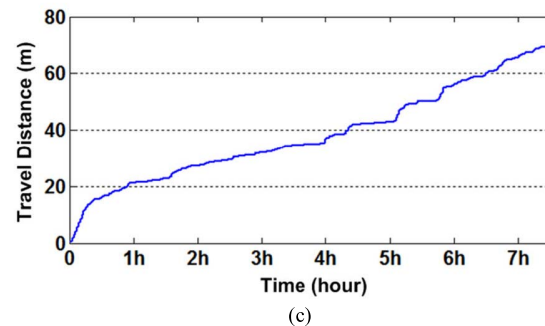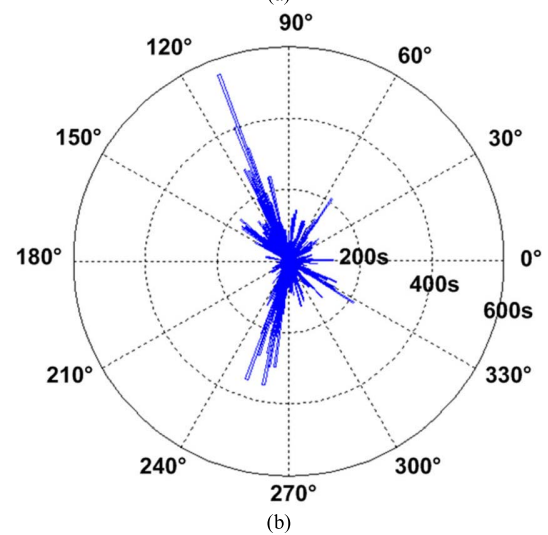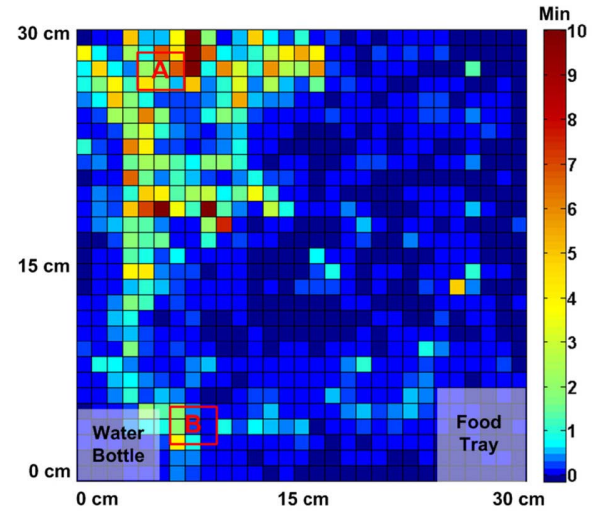
Fig. 14. *In vivo* experimental results showing the automated tracking for the LED/body during $\sim$7 hrs of the experiment inside the homecage: (a) the position of the mobile unit based on the LED tracking, (b) the distributed time of the rat's orientation based on the LED/body tracking, and (c) the travel distance of the rat in the homecage.

Fig. 10 shows the mobile unit prototype including the PMIC, an nRF MCU, and an LED. The PMIC was fabricated in the TSMC 0.35-μm 4M2P standard CMOS process, and it occupies 3.5 mm^2 of silicon area. The mobile unit includes L_3 and L_4 coils, which specifications are given in Table I, at the bottom of the box, a small PCB with the PMIC wirebonded to a QFN package, and a separate PCB with nRF MCU, RF matching network, 2.4 GHz monopole

TABLE II
BENCHMARKING WIRELESSLY-POWERED SYSTEMS FOR BEHAVIORAL EXPERIMENTS

Year of publication	2012 [16] 2014 [19]	2014 [20]	2013 [21]	2014 [22]	2014 [23]	**This work**
Frequency	13.56 MHz	13.56 MHz	1.55 MHz	2.457 MHz	13.56 MHz	**13.56 MHz**
Coil coupling	3-/4- coil	4 coil	2 coil	4 coil	2 coil	**3/4 coil**
Tx coil type	PSC array	PSC array	PSC array	WWC	PSC	**WWC**
Number of power amplifiers	27	1	16	1 or 2	1	**1**
Powered experimental area	51.5×45 cm^2	30×30 cm^2	45×26 cm^2	15×20 cm^2	18×34 cm^2	**30×30 cm^2**
Rx power	20 mW	*115 mW	~ 22 mW	N/A	1.7 mW	**24 mW**
Rx coil diameter (L_3, L_4)	4 cm, 2.5 cm	4.2 cm, 1.1 cm	4 cm	1.9 cm, 1.6 cm	1.2 cm	**2.5 cm, 1 cm**
Efficiency (Distance)	$\sim 21\%$ (7cm)	*76% (4cm)	**7.2% (10 cm)	***10% (7 cm)	17% (3 cm)	**21.9% (7cm)**
Animal subject tracking (Resolution)	Position (N/A)	N/A	Position (N/A)	N/A	Position (1 cm)	**Position & Orientation (1.6 cm)**
Tracking Method	Magnetic	N/A	Impedance	N/A	Magnetic Field	**Infrared/RGB**
Closed loop control	Yes	N/A	N/A	Yes	Yes	**Yes**
Automatic resonance tuning	N/A	N/A	N/A	N/A	N/A	**Yes**
In vivo experiment (duration)	Yes (1 hr)	N/A	N/A	Yes (N/A)	N/A	**Yes (7 hr 20 min)**

*Source resistance is 1 Ω. ** Estimated *** Single PA is used*

antenna, and the LED indicator. The total weight of the mobile unit in this prototype was 16.2 g including the weight of the box, which was 9.1 g.

VI. MEASUREMENT RESULTS

Fig. 11 shows the measured PTE distribution between the Tx and Rx coils inside the EnerCage-HC at $d_{23} = 7$ cm based on the direct PTE measurement procedure in [40], using a network analyzer across the inductive links. The surface of homecage was marked by a checker board with 3 cm resolution for the PTE measurements. At the corners, the maximum measured PTE was 36.3%, which matches very well with the simulated result in Fig. 5b. The lowest and average PTEs across the homecage were 16.1% and 21.9%, respectively. The efficiency of the PA was measured 81% at $V_{DD\_Tx} = 4.5$ V, and gradually decreased to 63% at $V_{DD\_Tx} = 20$ V, which is the maximum voltage in this prototype EnerCage-HC system.

The maximum permissible exposure (MPE) to magnetic field strength based on the IEEE standard is $16.3/f_c$ (A/m), where f_c is in MHz, resulting in the equivalent maximum power density at 13.56 MHz to be 54.3 mW/cm^2 [46]. Since the WWC at the bottom of the EnerCage (L_1) has 17 cm $\times$ 17 cm $= 289$ cm^2 area, the maximum safe power transmission level would be 15.6 W. However, the maximum transmitted RF power in the current EnerCage-HC prototype is 4.4 W, and it only happens over a short period in the worst case scenario when the animal stands up. This is equivalent to a maximum power density of 15.2 mW/cm^2, which is well below the safety limit. Therefore, the EnerCage-HC system satisfies the IEEE standard with respect to safe level of human or animal exposure to radio frequency electromagnetic fields [46].

Fig. 12 shows the *in vivo* experimental setup for the EnerCage-HC prototype. The animal subject was a one-year-old rat weighting 300 g. The mobile unit was placed in the plastic box in Fig. 10 and attached to a special jacket, designed for rats. All experiments were conducted with the prior approval from the Institutional Animal Care and Use Committee (IACUC) at the Georgia Institute of Technology. During the experiment, the GUI reported the real-time video, V_{RECP}, V_{DD_Tx}, and the LED/Body tracking information along with the rat body orientation and travelled distance. Water bottle and food dispenser were also placed in the homecage for the 7 hr and 20 min experiment, during which the rat was freely moving in the homecage.

Fig. 13 shows the measured V_{RECP} and V_{DD_Tx} during 7 hours and 20 min without any interruption. The EnerCage-HC continuously delivered 24 mW of regulated power to the mobile unit by maintaining V_{RECP} constant at 2.3 V, which was high enough for the LDO to generate a stable $V_{DD} = 2$ V, thanks to the CPCL module. The V_{DD_Tx} was dynamically adjusted by the CPCL module in the EnerCage-HC between 4.5 V and 20 V corresponding to the PA power consumption of 0.3 W to 7 W, depending on the coil separation, d_{23}. We should point out that the 7 W power consumption in the PA is the worst case scenario of animal standing up, which is maximum coil separation or angular misalignment of the Rx coil. Fig. 13 inset shows that the CPCL increased V_{DD_Tx}, when the rat moved to low PTE areas or stood up on his hind limbs ($t < 14817$ s), and decreased V_{DD_Tx} when the mobile unit was close to the homecage surface or high PTE areas ($t > 14817$ s). The mobile unit received stable power inside the homecage during 7:20 hr of continuous operation regardless of the animal movements, proving the functionality of the EnerCage-HC.

Fig. 14 shows the measured tracking information including the position and orientation of the animal inside the homecage during the 7:20 hr *in vivo* experiment. Fig. 14a shows the automated position data for the LED indicator on the mobile unit. The heat map shows how long the animal spent in a certain location. The statistical result for the rat's orientation based on the automated LED/body tracking data is shown in Fig. 14b. Since most of the time the rat moved across the left corners, marked A and B in Fig. 14a, the orientation of the rat shows peaks in those directions. The rat's travel distance based on the LED tracking data is shown in Fig. 14c,

which indicates that the rat moved about 69.6 m in the homecage during the experiment.

Table II compares the EnerCage-HC system with the previous attempts at developing wirelessly-powered systems for behavioral experiments on small freely behaving animals. The presented EnerCage-HC, 1) provides the largest wirelessly-powered area per one PA with the proposed slanted multi-coil WWC arrangement, 2) is the only system equipped with accurate 2D/3D animal subject tracking, not only for real time coil switching but also for the behavioral analysis of the subject, 3) compared to [19], the customized mobile unit provides higher average power efficiency with smaller Rx coils at 7 cm distance, thanks to its ART mechanism. It also ensures safe operation against frequent over voltage situations along with robust and smooth closed-loop control during long-term *in vivo* experiments, improving the quality of the collected biosignal and behavioral data.

VII. Conclusion

A novel wireless platform for electrophysiology experiments inside the standard homecage has been presented. This system, called the EnerCage-HC, takes advantage of multi-coil coupling and Kinect® based optical localization to offer an efficient and low-cost technology for wireless powering any electronics attached to a small animal subject and track its behavior. The EnerCage-HC includes four switchable slanted triangular WWCs covering lower corners of the homecage by establishing 4-coil power transfer as well as a square-shaped WWC at the bottom of the cage for 3-coil power transfer in the center. The Kinect tracking algorithm is key to achieve the switchable 3-/4-coil function, which in turn allows the use of only one PA in the system, which significantly reduces the system complexity, cost, and heat dissipation. The 3-/4-coil mechanism achieves three times higher and more homogeneous PTE in the homecage compared to the conventional single WWC. A PMIC is used in the mobile unit to offer high efficiency voltage rectification/regulation, and communication between mobile and stationary units for closed-loop power control. The functionality of the EnerCage-HC prototype was demonstrated in both bench-top and *in vivo* experiments. The mobile unit was attached to a rat, and continuously received 24 mW of regulated power during a 7:20 hour experiment, while a Kinect® installed 90 cm above the homecage tracked the animal position and orientation with 1.6 cm accuracy. To the best of our knowledge, the EnerCage-HC system is the first wirelessly powered cage equipped with the tracking functions for both animal position and orientation. It has the ability to create an automated enriched environment inside standard homecage for long-term electrophysiology experiments.

Acknowledgment

The authors would like to thank Dr. L. O'Farrell and members of the GT-Bionics Lab for their advice and help with the benchtop measurements and *in vivo* experiments.

References

[1] J. R. Manns and H. Eichenbaum, "A cognitive map for object memory in the hippocampus," *Learn. Memory*, vol. 16, no. 10, pp. 616–624, Sep. 2009.

[2] Y. Choi, S. Park, Y. Chung, R. K. Gore, A. W. English, and R. V. Bellamkonda, "PDMS microchannel scaffolds for neural interfaces with the peripheral nervous system," in *Proc. IEEE 27th Int. Conf. Micro Electro Mech. Syst. (MEMS)*, Jan. 2014, pp. 873–876.

[3] A. M. Sodagar, G. E. Perlin, Y. Yao, K. Najafi, and K. D. Wise, "An implantable 64-channel wireless microsystem for single-unit neural recording," *IEEE J. Solid-State Circuits*, vol. 44, no. 9, pp. 2591–2604, Sep. 2009.

[4] T. A. Szuts *et al.*, "A wireless multi-channel neural amplifier for freely moving animals," *Nature Neurosci.*, vol. 14, no. 2, pp. 263–269, Feb. 2011.

[5] E. Greenwald, M. Mollazadeh, C. Hu, W. Tang, E. Culurciello, and N. V. Thakor, "A VLSI neural monitoring system with ultra-wideband telemetry for awake behaving subjects," *IEEE Trans. Biomed. Circuits Syst.*, vol. 5, no. 2, pp. 112–119, Apr. 2011.

[6] D. Fan *et al.*, "A wireless multi-channel recording system for freely behaving mice and rats," *PLoS One*, vol. 6, no. 7, pp. e22033-1–e22033-9, Jul. 2011.

[7] S. B. Lee, M. Yin, J. R. Manns, and M. Ghovanloo, "A wideband dual-antenna receiver for wireless recording from animals behaving in large arenas," *IEEE Trans. Biomed. Eng.*, vol. 60, no. 17, pp. 1993–2004, Jul. 2013.

[8] R. R. Harrison *et al.*, "A low-power integrated circuit for a wireless 100-electrode neural recording system," *IEEE J. Solid-State Circuits*, vol. 42, no. 1, pp. 123–133, Jan. 2007.

[9] D. J. Guggenmos *et al.*, "Restoration of function after brain damage using a neural prosthesis," *Proc. Nat. Acad. Sci. USA*, vol. 110, no. 52, pp. 21177–21182, Dec. 2013.

[10] R. E. Millard and R. K. Shepherd, "A fully implantable stimulator for use in small laboratory animals," *J. Neurosci. Methods*, vol. 166, no. 2, pp. 168–177, Nov. 2007.

[11] B. Lenaerts and R. Puers, "Inductive powering of a freely moving system," *Sens. Actuators A, Phys.*, vols. 123–124, pp. 522–530, Sep. 2005.

[12] P. Cong, N. Chaimanonart, W. Ko, and D. Young, "A wireless and batteryless 130 mg 300 μW 10 b implantable blood-pressure-sensing microsystem for real-time genetically engineered mice monitoring," in *IEEE Int. Solid-State Circuits Conf.-Dig. Tech. Papers*, Feb. 2009, pp. 428–429.

[13] Starr Life Sciences Corp. *VitalView Animal Monitoring Products*. [Online]. Available: http://starrlifesciences.com/, accessed May 17, 2015.

[14] Triangle Biosystems International Corp. *W-Series*. [Online]. Available: http://www.trianglebiosystems.com/, accessed May 17, 2015.

[15] C. T. Wentz, J. G. Bernstein, P. Monahan, A. Guerra, A. Rodriguez, and E. S. Boyden, "A wirelessly powered and controlled device for optical neural control of freely-behaving animals," *J. Neural Eng.*, vol. 8, no. 4, p. 046021, Jun. 2011.

[16] U.-M. Jow, M. Kiani, X. Huo, and M. Ghovanloo, "Towards a smart experimental arena for long-term electrophysiology experiments," *IEEE Trans. Biomed. Circuits Syst.*, vol. 6, no. 5, pp. 414–423, Oct. 2012.

[17] D. M. Russell, D. McCormick, A. J. Taberner, S. C. Malpas, and D. M. Budgett, "A high bandwidth fully implantable mouse telemetry system for chronic ECG measurement," in *Proc. Annu. Int. Conf. IEEE Eng. Med. Biol. Soc.*, Aug./Sep. 2011, pp. 7666–7669.

[18] Millar, Inc. *TRM Implantable Telemetry System*. [Online]. Available: http://millar.com/products/telemetry, accessed May 17, 2015.

[19] U.-M. Jow, P. McMenamin, M. Kiani, J. R. Manns, and M. Ghovanloo, "EnerCage: A smart experimental arena with scalable architecture for behavioral experiments," *IEEE Trans. Biomed. Eng.*, vol. 61, no. 1, pp. 139–148, Jan. 2014.

[20] S. A. Mirbozorgi, H. Bahrami, M. Sawan, and B. Gosselin, "A smart multicoil inductively coupled array for wireless power transmission," *IEEE Trans. Ind. Electron.*, vol. 61, no. 11, pp. 6061–6070, Nov. 2014.

[21] N. Soltani, M. S. Aliroteh, and R. Genov, "Cellular inductive powering system for weakly-linked resonant rodent implants," in *Proc. IEEE BioCAS Conf.*, Oct./Nov. 2013, pp. 350–353.

[22] K. Eom *et al.*, "A wireless power transmission system for implantable devices in freely moving rodents," *Med. Biol. Eng. Comput.*, vol. 52, no. 8, pp. 639–651, Jun. 2014.

[23] E. G. Kilinc, G. Conus, C. Weber, B. Kawkabani, F. Maloberti, and C. Dehollain, "A system for wireless power transfer of micro-systems in-vivo implantable in freely moving animals," *IEEE Sensors J.*, vol. 14, no. 2, pp. 522–531, Feb. 2014.

[24] L. H. Tecott and E. J. Nestler, "Neurobehavioral assessment in the information age," *Nature Neurosci.*, vol. 7, no. 5, pp. 462–466, May 2004.

[25] V. H. Denenberg, "Open-field behavior in the rat: What does it mean?" *Ann. New York Acad. Sci.*, vol. 159, pp. 852–859, Jul. 1969.

[26] R. L. Clarke, R. F. Smith, and D. R. Justesen, "An infrared device for detecting locomotor activity," *Behavior Res. Methods, Instrum., Comput.*, vol. 17, no. 5, pp. 519–525, Sep. 1985.

[27] C. J. Twining, C. J. Taylor, and P. Courtney, "Robust tracking and posture description for laboratory rodents using active shape models," *Behavior Res. Methods, Instrum., Comput.*, vol. 33, no. 3, pp. 381–391, Aug. 2001.

[28] B. M. Spruijt and L. DeVisser, "Advanced behavioural screening: Automated home cage ethology," *Drug Discovery Today, Technol.*, vol. 3, no. 2, pp. 231–237, 2006.

[29] D. H. Godden and D. Graham, "'Instant' analysis of movement," *J. Experim. Biol.*, vol. 107, pp. 505–508, Nov. 1983.

[30] L. P. J. J. Noldus, A. J. Spink, and R. A. J. Tegelenbosch, "EthoVision: A versatile video tracking system for automation of behavioral experiments," *Behavior Res. Methods, Instrum., Comput.*, vol. 33, no. 3, pp. 398–414, Aug. 2001.

[31] S. Kato, K. Tamada, Y. Shimada, and T. Chujo, "A quantification of goldfish behavior by an image processing system," *Behavioural Brain Res.*, vol. 80, nos. 1–2, pp. 51–55, Oct. 1996.

[32] S. N. Fry, M. Bichsel, P. Müller, and D. Robert, "Tracking of flying insects using pan-tilt cameras," *J. Neurosci. Methods*, vol. 101, no. 1, pp. 59–67, Aug. 2000.

[33] J. Chrásková, Y. Kaminsky, and I. Krekule, "An automatic 3D tracking system with a PC and a single TV camera," *J. Neurosci. Methods*, vol. 88, no. 2, pp. 195–200, May 1999.

[34] T.-H. Ou-Yang, M.-L. Tsai, C.-T. Yen, and T.-T. Lin, "An infrared range camera-based approach for three-dimensional locomotion tracking and pose reconstruction in a rodent," *J. Neurosci. Methods*, vol. 201, no. 1, pp. 116–123, Sep. 2011.

[35] E. Whitmire, T. Latif, and A. Bozkurt, "Kinect-based system for automated control of terrestrial insect biobots," in *Proc. 35th Annu. Int. Conf. IEEE EMBS*, Jul. 2013, pp. 1470–1473.

[36] Tecniplast Corp. *Sealsafe Plus Rat.* [Online]. Available: http://www.tecniplast.it/, accessed May 17, 2015.

[37] M. Kiani and M. Ghovanloo, "An RFID-based closed-loop wireless power transmission system for biomedical applications," *IEEE Trans. Circuits Syst. II, Exp. Briefs*, vol. 57, no. 4, pp. 260–264, Apr. 2010.

[38] H.-M. Lee, K.-Y. Kwon, W. Li, and M. Ghovanloo, "A power-efficient switched-capacitor stimulating system for electrical/optical deep-brain stimulation," in *IEEE Int. Solid State Circuits Conf. Dig. Tech. Papers*, Feb. 2014, pp. 414–415.

[39] A. Kurs, A. Karalis, R. Moffatt, J. D. Joannopoulos, P. Fisher, and M. Soljačić, "Wireless power transfer via strongly coupled magnetic resonances," *Science*, vol. 317, pp. 83–86, Jul. 2007.

[40] M. Kiani, U.-M. Jow, and M. Ghovanloo, "Design and optimization of a 3-coil inductive link for efficient wireless power transmission," *IEEE Trans. Biomed. Circuits Syst.*, vol. 5, no. 6, pp. 579–591, Dec. 2011.

[41] L. L. Chen, L.-H. Lin, C. A. Barnes, and B. L. McNaughton, "Head-direction cells in the rat posterior cortex," *Experim. Brain Res.*, vol. 101, no. 1, pp. 24–34, Sep. 1994.

[42] J. L. Calton and J. S. Taube, "Degradation of head direction cell activity during inverted locomotion," *J. Neurosci.*, vol. 25, no. 9, pp. 2420–2428, Mar. 2005.

[43] M. A. P. Moita, S. Rosis, Y. Zhou, J. E. LeDoux, and H. T. Blair, "Hippocampal place cells acquire location-specific responses to the conditioned stimulus during auditory fear conditioning," *Neuron*, vol. 37, no. 3, pp. 485–497, Feb. 2003.

[44] B. Lee, M. Kiani, and M. Ghovanloo, "A triple-loop inductive power transmission system for biomedical applications," *IEEE Trans. Biomed. Circuits Syst.*, 2015, doi: 10.1109/TBCAS.2014.2376965.

[45] H.-M. Lee and M. Ghovanloo, "An integrated power-efficient active rectifier with offset-controlled high speed comparators for inductively powered applications," *IEEE Trans. Circuits Syst. I, Reg. Papers*, vol. 58, no. 8, pp. 1749–1760, Aug. 2011.

[46] *IEEE Standard for Safety Levels With Respect to Human Exposure to Radio Frequency Electromagnetic Fields, 3 kHz to 300 GHz*, IEEE Standard C95.1-1991, 1992.

Byunghun Lee (S'11) received the B.S. degree from Korea University, Seoul, Korea, in 2008, and the M.S. degree from the Korea Advanced Institute of Technology (KAIST), Daejeon, Korea, in 2010. He is currently pursuing the Ph.D. degree in electrical and computer engineering at the Georgia Institute of Technology. From 2010 to 2011, he was involved in wireless power transfer systems at KAIST as a Design Engineer. His research interests include analog/mixed-signal IC design and wireless power transfer systems for biomedical applications.

Mehdi Kiani (S'09) received the B.S. degree from Shiraz University, Shiraz, Iran, in 2005, the M.S. degree from the Sharif University of Technology, Tehran, Iran, in 2008, and the M.S. and Ph.D. degrees in electrical and computer engineering from the Georgia Institute of Technology, in 2012 and 2013, respectively. He is currently an Assistant Professor with the Department of Electrical Engineering, Pennsylvania State University. His research interest is integrated circuits and systems design for bio application. He was a recipient of the Georgia Tech Sigma Xi Best Ph.D. Thesis Award, and Georgia Tech Chih Foundation Research Award for excellent research in the fields of engineering and health sciences.

Maysam Ghovanloo (S'00–M'04–SM'10) received the B.S. degree in electrical engineering from the University of Tehran, Tehran, Iran, in 1994, the M.S. degree in biomedical engineering from the Amirkabir University of Technology, Tehran, in 1997, and the M.S. and Ph.D. degrees in electrical engineering from the University of Michigan, Ann Arbor, MI, USA, in 2003 and 2004, respectively. From 2004 to 2007, he was an Assistant Professor with the Department of Electrical and Computer Engineering, NC-State University, Raleigh, NC. He joined the Faculty of the Georgia Institute of Technology, Atlanta, GA, USA, in 2007, where he is currently an Associate Professor and the Founding Director of the GT-Bionics Laboratory, School of Electrical and Computer Engineering. He has authored or co-authored over 150 peer-reviewed publications. He is a member of the Tau Beta Pi, the American Association for the Advancement of Science, Sigma Xi, the IEEE Solid-State Circuits Society, the IEEE Circuits and Systems Society, and the IEEE Engineering in Medicine and Biology Society. He was the 2010 recipient of a CAREER Award from the National Science Foundation. He has organized several special sessions and was a member of the Technical Program Committees for major conferences in the areas of circuits, systems, sensors, and biomedical engineering. He served on the Imagers, MEMS, Medical, and Displays Subcommittee of the International Solid-State Circuits Conference from 2010 to 2014. He is also an Associate Editor of the IEEE TRANSACTIONS ON BIOMEDICAL ENGINEERING and the IEEE TRANSACTIONS ON BIOMEDICAL CIRCUITS AND SYSTEMS.